SOLID–SOLID INTERFACIAL DYNAMICS AND MODELLING

WEI CHEN, LITENG YANG, LIMEI CAO & XINGHUI SI
University of Science and Technology Beijing, China

ABSTRACT

Solid interface modelling is critical to the stability, stiffness, deformation and thermal performance of a structural system. Different from interior elements, a boundary element may experience changes in material properties, loads and dynamic modes. To date, the computational results from boundary elements are less satisfactory, and the strategy to overcome that drawback is to increase the mesh density near the boundary elements or significantly reduce the time steps when dynamic loads are applied. Recently, new insight into physics has revealed that a solid−solid interface may experience nondissipative dynamics and produce nodes, antinodes and saddles dynamically. Instead of increasing the mesh density and time step, we propose explicitly including the physics of nondissipative dynamics in the finite element models to reduce the overall demands and cost of computing. In this work, we present the differential equations of nondissipative dynamics and mathematical formulas for computing nodes, antinodes and saddles, which are readily coded in any finite element software. We will show the details of the derivations of those formulas and how they can be included in the finite element models. We will also show some canonical calculations for saving computational time and model sizes and compare the results with measurements and the sensitivity to the mesh density and time steps. We expect that the revelation of new physics and mathematical formulas will increase the accuracy and efficiency of simulations for industrial applications.

Keywords: interfacial phenomena, nondissipative dynamics, solid mechanics, speed of the first sound, speed of the second sound, pulses at interface, pulse train at interface, chaos.

1 INTRODUCTION

A solid–solid interface is a basic mechanical structure, which can be found in almost every engineering application of mechanical structures. Hence, the accurate prediction of stress field, elastic variation and plastic deformation on an interface is important to the design, manufacture and operation of a machinery. To carry out the computational modelling, a numerical or computational scheme such as the finite element method (FEM) and the boundary element method (BEM) has to be chosen and the corresponding algorithm has to be coded and executed in a computational resource. Although the stress field are readily resolvable inside the solid domains, the interfacial damages and deformation have shown the substantial discrepancies between the theoretical prediction and the lab observations. In order to resolve the disparity, the significant effort has been made to develop sophisticated numerical schemes such as BEM. As the result, BEM is particularly suited for the interfacial phenomena because only discretisation of surfaces is necessary; hence, it can adapt to any complexity of surface topologies in a contact. Additionally, the sensitive, oscillatory differential equations at an interface can be applied and solved with high precision algorithms [1]. However, due to the assumptions made on the integral equations and the coupling of the normal and tangential components of stress and strain at the contact, the calculation of plastic deformation, sliding and strain rates still deviates from observations [2]. Recently, the theory on the isentropic motion in solids has shed some lights on the hydrodynamic anomalies in the motion of solids. One of outcomes from the theory of excess entropy or isentropic motion is the interfacial effects, which means that under the oscillatory loads, the interface resonates and generates sound. Acoustic propagation creates a discontinuity of field variables across

WIT Transactions on Engineering Sciences, Vol 136, © 2024 WIT Press
www.witpress.com, ISSN 1743-3533 (on-line)
doi:10.2495/BE470081

an interface. The interfacial phenomena are strongly dependent on this nondissipative dynamics. In this work, we give an introduction on this new theory and present the validation by comparing it with the experimental data. Through the mathematical derivation and experimental data validation, we hope to supply the formulas that can be used in the calculation of strain and stress field without additional burden on the finite element method and computation.

The solid–solid interface has been considered as the multiscale problem [3], [4]. For the historical reasons, the interfacial problems have been dealt with each discipline such as heat transfer, mechanical and electrical issues [3], [5]–[7]. The essence of the theoretical work has been more or less focused on the geometrical distribution of the contact. When two nominally perfect surfaces are in contact, the interface is assumed to be separated by many geometrical spikes and non-uniformities such that the contact is only partially in physical contact. These protrusions have random shapes and sizes and the stress and strain on the interface therefore depends on the distribution statistically [8]. Such treatment of contact surfaces has been known to employee a parameter called roughness and it has been found that the roughness alone is not sufficient to describe the mechanical stiffness for the texture effects [9]. The thermal performance of an interface has been related to the so-called interface thermal conductance where an additional temperature step has been observed. This phenomenon has been called Kapitza conductance to celebrate his discovery in the early 20th century [10]. Initially, the interface thermal conductance has been thought as the phenomenon particularly for Helium at low temperature [11]. Later, the interfacial temperature differences have been found in many solid–solid interfaces and the connection to the speed of sound has been established [6]. The interfacial electric conductance has also been observed and another phenomenon associated with the interfacial conductance is the so-called tunnelling effect [12]. Although the thermal-electron tunnelling phenomena have been observed over a wide range of materials, there is few on the possible tunnelling phenomenon in the mechanical behaviour [13], where the tunnelling effect has been studied by the quantum effect while the interfacial effect is not. Overall, while some significant progress on the interfacial phenomena has been made in applications, a coherent theory and mathematical models are not yet available to consolidate various theories and models.

When the finite element method becomes available, the expectation was high to address the interfacial issues [14]; however, the challenges faced by FEM left an opportunity for the development of BEM [1], [8], [15], [16]. The principle of BEM is to ‘discretising’ a volumetric domain into matrices and fitting the exact boundary conditions to the domain matrices through integral equations casted by the Green’s functions, which is advantageous over other computational methods on the accuracy of the solutions on the boundaries [17]. However, the applications and experiences have exposed some shortcomings and difficulties at interfaces [2], [18]–[20].

The interfacial mechanical property is an old scientific field dated back to da Vinci era [21]. The interfacial science relates to many subjects such as physics, chemistry, material science, biology, and engineering. The pioneers of tribology rely on the concept of friction from the roughness or asperity of interfaces [22]. In the classical tribology, the work to properly account for the loss of energy and increase of resistance has been weighted on the interpretation of distribution of real contact areas. The direct consequences of the friction are then the wearing of contact areas accompanied with the sound [23]. In addition to the plastic deformation and acoustic emission, the researches on tribology have revealed that the responses of the sliding interfaces are strong function of time [24], [25]. The so-called rigid modes are included on the interaction of the primary structure motions with the non-classically damped modal properties [26].

It is almost impossible to judge whether the advances in the theoretical fronts and the meshing techniques have unlocked the mystery of interfacial phenomena. However, one thing is clear that the developments, regardless of the theoretical, numerical or experimental work, are exploratory and fragmented in nature. In other words, we may have not yet lodged on a coherent physics of interfacial phenomena. Recently, a study on the nondissipative dynamics hypothesises that in any periodic motion, the dissipative and nondissipative dynamics coexists with their own laws of motion [27]. With that theory, the temperature discontinuity at interfaces has been associated with the speed of the first and the second sound. Moreover, the predicted temperature profile on the sites of excitation at the interface has been compared to the experimental measurements. The theory assumes that in one period, there shall be at least one point in time that entropy in the zero. At that particular point, we must employee the governing equations for nondissipative motion instead of the dissipative process. When a solid pocket follows the nondissipative dynamics, many new behaviours and physics are exposed, which may lead to the resolution of the interfacial phenomena.

In this work, we follow the approach of nondissipative dynamics, formulate the motion of solids at the interface and validate it with the experimental data. The formulas can be used to calculate the interfacial plastic deformation and friction resistance incurred. The article is organised in the following order. First, we separate the nondissipative motion from the dissipative motion in an isotropic, Hookean solid. Second, we establish the boundary conditions for the nondissipative motions of solids. Then, we solve the velocity on a two-dimensional interface and validate it with the experimental data. We end our study with a short conclusion.

2 ISENTROPIC AND ENTROPIC MOTIONS

In this section, we develop a means to separate nondissipative motion from the dissipative motion.

The purpose is that the isentropic motion follows the different physics of separating the isentropic motion from the entropic motion. In the modern theoretical physics and fluid mechanics, a nondissipative motion is ideal and does not exist in reality; however, in the theory of isentropic dynamics, the nondissipative motion actually exist and represents a different thermodynamic state and there is a conversion between entropic solid and isentropic solid. When an oscillatory load is applied, an isentropic motion can excite the domain of interest and result in the resonance and generate sounds. On the contrary, a theoretical nondissipative solid never goes beyond the limit of an entropic solid; moreover, the nondissipative solid has little to do with acoustics and supersolid that we will discuss with next.

In this work, we start with the governing equations of isotropic, linear, elastic, Hookean solid in three dimensional motions in spatiotemporal [28], [29]:

$$\frac{D\rho}{Dt} + \rho\, \nabla \cdot \mathbf{u} = 0 \tag{1}$$

$$\rho \frac{D\mathbf{u}}{Dt} = \nabla \cdot \Xi \tag{2}$$

$$\rho \frac{Dh}{Dt} = \Xi : \Lambda - \nabla \cdot \mathbf{q} \tag{3}$$

where ρ, h, $\mathbf{u}$, $\mathbf{q}$, Ξ and Λ are the density, enthalpy, velocity and heat flux vectors, stress and rate of deformation tensors, respectively. Here, we note the equivalence of the local and instant velocity gradient, strain rate and the rate of deformation. Consequently, the stress tensor is followed by the constitutive relation of the Hooke's law,

$$\Xi_{ij} = -p\delta_{ij} + \lambda\mathcal{E}_{kk}\delta_{ij} + 2\mu\mathcal{E}_{ij} \tag{4}$$

where p is the hydrostatic pressure, δ_{ij} is the Kronecker symbol, $\mathcal{E}_{ij}$ is the strain deviator tensor and λ and μ are the Lame constants, which relate to the more familiar shear modulus G, Young's modulus E and Poisson ratio υ by

$$\mu = G = \frac{E}{2(1+\upsilon)} \quad \text{and} \quad \lambda = \frac{\upsilon E}{(1+\upsilon)(1-2\upsilon)} \tag{5}$$

The rate of deformation tensor can be expressed by

$$\Lambda = \Lambda_{ij} = \frac{1}{2}\left(\frac{\partial u_i}{\partial x_j} + \frac{\partial u_j}{\partial x_i}\right) \tag{6}$$

For an isotropic, elastic solid, we adopt the Venant–Beltrami theorem [29] and find that the deviators of the strain tensor $\mathcal{E}_{ij}$ are traceless, i.e. the normal stress $\mathcal{E}_{kk} = 0$ [29]. The strain deviator tensor $\mathcal{E} = \mathcal{E}_{ij}$ then follows by

$$\mathcal{E} = \mathcal{E}_{ij} = \frac{1}{2}\left(\frac{\partial \xi_i}{\partial x_j} + \frac{\partial \xi_j}{\partial x_i}\right) \; i \neq j \tag{7}$$

From the thermodynamic relation,

$$h = e + \frac{p}{\rho} \tag{8}$$

where e is the specific mass density of internal energy. Bring (4), (6) and (8) into (3) and utilise (1),

$$\rho\frac{De}{Dt} = -pI:\Lambda + 2\mu\mathcal{E}:\Lambda - \nabla\cdot\mathbf{q} \tag{9}$$

From the thermodynamic relation of the internal energy on temperature,

$$\rho\frac{De}{Dt} = \rho c_v\frac{DT}{Dt} + \left[T\left(\frac{\partial p}{\partial T}\right)_\rho - p\right]\frac{\partial u_i}{\partial x_i} \tag{10}$$

(10) can be expressed by temperature,

$$\rho c_v\frac{DT}{Dt} = -pI:\Lambda + 2\mu\mathcal{E}:\Lambda - \nabla\cdot\mathbf{q} + \left[p - T\left(\frac{\partial p}{\partial T}\right)_\rho\right]\frac{\partial u_i}{\partial x_i} \tag{11}$$

The thermodynamic relation of the internal energy on temperature, entropy, pressure and specific volume yields

$$de = Tds + pdv \tag{12}$$

or

$$\frac{De}{Dt} = T\frac{Ds}{Dt} + p\frac{Dv}{Dt} = T\frac{Ds}{Dt} - \frac{p}{\rho^2}\frac{D\rho}{Dt} \tag{13}$$

With (13), (11) becomes

$$\rho T\frac{Ds}{Dt} - \frac{p}{\rho}\frac{D\rho}{Dt} = -p\frac{\partial u_i}{\partial x_i} + 2\mu\mathcal{E}:\Lambda - \nabla\cdot\mathbf{q} \tag{14}$$

With the continuity eqn (1), the energy conservation is expressed by the local mass density of entropy,

$$\rho T\frac{Ds}{Dt} = 2\mu\mathcal{E}:\Lambda - \nabla\cdot\mathbf{q} \tag{15}$$

Here, we introduce a new variable, excess entropy δs

$$\delta s = s_0 - s \tag{16}$$

where s and s_0 are the local mass density of the solid and the mean entropy of the domain of interest. Since it is a constant, we may assume that s_0 is the entropy of the nondissipative process, and when $s = s_0$, the local solid parcel experiences a nondissipative process isentropically. The excess entropy divides a solid domain into two thermodynamic domains: the entropic or dissipative domain and the isentropic or nondissipative domain. Excess entropy is a local quantity and can be determined by (15)

$$\rho T \frac{D\delta s}{Dt} = \nabla \cdot \mathbf{q} - 2\mu \mathcal{E} : \Lambda \tag{17}$$

When $\nabla \cdot \mathbf{q} = 0$ and $2\mu \mathcal{E} : \Lambda = 0$, (17) says

$$\frac{D\delta s}{Dt} = 0 \text{ or } \delta s = 0 \tag{18}$$

Note that we replace $\delta s = C$ by an integral constant C to keep $\delta s = 0$. In other words, we have established criterion (18) to discern local solid on whether it is a regular solid or supersolid. The compliance of the excess entropy to the Clausius–Duhem's law is given in Chen [30].

It is necessary to explain the physical importance of (18) to the momentum eqn (2). For example, the functions of the strain tensor and heat flux depend on time by

$$\mathcal{E} = \mathcal{E}_{ij} = \cos \omega t \, \hat{\mathcal{E}}_{ij} \tag{19}$$

and

$$\mathbf{q} = \cos \omega t \, \hat{\mathbf{q}} \tag{20}$$

When $\cos \omega t = 0$, from (19) and (20), (17) yields

$$\frac{D\delta s}{Dt} = 0 \tag{21}$$

and the momentum conservation (2) yields

$$\rho \frac{D\mathbf{u}}{Dt} = -\nabla \cdot p \tag{22}$$

Therefore, we conclude that the governing equations for a nondissipative solid have the form of

$$\frac{D\rho}{Dt} + \rho \, \nabla \cdot \mathbf{u} = 0 \tag{23}$$

$$\rho \frac{D\mathbf{u}}{Dt} = -\nabla \cdot p \tag{24}$$

$$\rho \frac{Dh}{Dt} = 0 \tag{25}$$

It is clear that the governing eqns (23)–(25) of a nondissipative solid or supersolid are identical to the governing equations of the superfluid [31], as suggested [32], [33]. From the Maxwell relations in thermodynamics,

$$dp = \left(\frac{\partial p}{\partial \rho}\right)_s d\rho \tag{26}$$

Apply (26) to (23) and (24), and take the derivative with respect to the time, we have

$$\frac{1}{\left(\frac{\partial p}{\partial \rho}\right)_s}\frac{\partial p}{\partial t} + \bigtriangledown \cdot (\rho \mathbf{u}) = 0 \tag{27}$$

Take the derivative of (27) with respect to time,

$$\frac{1}{\left(\frac{\partial p}{\partial \rho}\right)_s}\frac{\partial^2 p}{\partial t^2} + \bigtriangledown \cdot \left[\rho \frac{\partial(\mathbf{u})}{\partial \mathrm{t}}\right] - \bigtriangledown \cdot [\mathbf{u} \bigtriangledown \cdot (\rho \mathbf{u})] = 0 \tag{28}$$

Take the divergence to (24), subtract it from (28), and rearrange,

$$\frac{\partial^2 p}{\partial t^2} - \left(\frac{\partial p}{\partial \rho}\right)_s \nabla^2 p = \Psi \tag{29}$$

where $\Psi = \left(\frac{\partial p}{\partial \rho}\right)_s \nabla \cdot (\rho \mathbf{u} \nabla \cdot \mathbf{u})$ is the nonlinear term. (29) is the wave equation for the momentum conservation of supersolid.

Take the derivative to (25) with respect to $\mathbf{x}$ and t and subtract the former from the latter,

$$\frac{\partial^2 T}{\partial t^2} - \mathbf{u} \cdot \mathbf{u} \nabla^2 T = \Phi \tag{30}$$

where $\Phi = -\frac{1}{\rho}\frac{\tilde{D}\boldsymbol{\rho}}{\tilde{D}t}\left(\frac{\partial T}{\partial t} + \mathbf{u} \cdot \boldsymbol{\nabla} T\right) + \frac{\tilde{D}\mathbf{u}}{\tilde{D}t}\boldsymbol{\nabla} T - \frac{\beta}{\rho}\frac{\tilde{D}T}{\tilde{D}t}\nabla \cdot \mathbf{u} + \frac{\beta \mathrm{T}}{\rho}\frac{\tilde{D}}{\tilde{D}t}(\nabla \cdot \mathbf{u})$ and $\beta = -\frac{1}{\hat{C}_V}\left(\frac{\partial p}{\partial T}\right)_V$. (30) is the wave equation for the energy conservation of supersolid.

From (29) and (30), we can construct a two-dimensional dynamical system (p, T) that

$$F(p,T) = \frac{\partial^2 p}{\partial t^2} - \left(\frac{\partial p}{\partial \rho}\right)_s \nabla^2 p \tag{31}$$

$$G(p,T) = \frac{\partial^2 T}{\partial t^2} - u^2 \nabla^2 T \tag{32}$$

At any arbitrary wavelets,

$$p = p_0 \sin(\mathbf{x} + \mathbf{c_1} t) \text{ and } T = T_0 \sin(\mathbf{x} + \mathbf{c_2} t) \tag{33}$$

where c_1 and c_2 are the characteristic speeds of the momentum and energy disturbances.

When the dynamical system experiences the disturbances of (33), (29) and (30) produce

$$F(p,T) = \frac{\partial^2 p}{\partial t^2} - \left(\frac{\partial p}{\partial \rho}\right)_s \nabla^2 p = -\left[c_1^2 - \left(\frac{\partial p}{\partial \rho}\right)_s\right] p = \Psi \tag{34}$$

$$G(p,T) = \frac{\partial^2 T}{\partial t^2} - u^2 \nabla^2 T = -[c_2^2 - u^2] T = \Phi \tag{35}$$

The nullified Jacobian of the dynamical system (34) and (35) yields the condition of resonance,

$$J = \begin{bmatrix} \frac{\partial F}{\partial p} & \frac{\partial F}{\partial T} \\ \frac{\partial G}{\partial p} & \frac{\partial G}{\partial T} \end{bmatrix} = -\begin{bmatrix} c_1^2 - \left(\frac{\partial p}{\partial \rho}\right)_s & 0 \\ 0 & c_2^2 - u^2 \end{bmatrix} = 0 \tag{36}$$

The condition for resonance of superfluid is given by (36) and calculated by Chen [34]

$$c_1^2 = \left(\frac{\partial p}{\partial \rho}\right)_s = \frac{E}{\rho} \tag{37}$$

and from $dT = \left(\frac{\partial T}{\partial \rho}\right)_s d\rho$ for an isentropic process,

$$c_2^2 = -\frac{R\rho}{M}\left(\frac{\partial T}{\partial \rho}\right)_s = \frac{R_s \alpha_p T}{\lambda_0 \kappa_T c_p \rho + \alpha_p^2 T} \tag{38}$$

where c_1 is the speed of the first sound and c_2 is the speed of the second sound. $R_s = \frac{R}{M}$ is the specific gas constant, κ_T is the isothermal compressibility, α_p is the isochoric thermal expansion coefficient, c_p is the isobaric specific heat and $\lambda_0 = 10^{-3}$. Some validation on the speed of the second sound can be found in Chen [27]. Another important result from the analysis of governing equations of the resonant solids are written as

$$\begin{cases} \rho\left(\frac{\partial \boldsymbol{u}}{\partial t} \pm \boldsymbol{c_1} \cdot \nabla \mathbf{u}\right) = -\nabla p \\ \rho\left(\frac{\partial \mathrm{T}}{\partial t} \pm \boldsymbol{c_2} \cdot \nabla \mathrm{T}\right) = 0 \end{cases} \tag{39}$$

Now, we have established the governing differential equations of supersolid (23), (24) and (25), resonant supersolid (39) from the governing differential equations of a Hookean solid (1), (2) and (3).

3 BOUNDARY OF THE SECOND LAW

In this section, we establish the initial and boundary conditions for the isentropic motions of a solid that are used to specify the integral constants in the solutions of supersolid and resonant supersolid.

From the theory of nondissipative dynamics, a regular solid and supersolid coexist dynamically and are mutually dependent and what connects and apportions them is the endless oscillatory motion; on the other hands, the existence of regular solid and supersolid sustains a perpetual motion. Therefore, the motion in regular solid activates supersolid and the velocity and temperature pass the momentum and energy from the regular solid to supersolid. The passing of mass, momentum and energy to supersolid can be described by the initial and boundary conditions on the boundary of the second law. These boundary conditions can be used to determine the coefficients from the general solutions of velocity and temperature in (39).

Quantitatively, when (16) is satisfied, the thermodynamic state of solid changes from entropic to isentropic, the governing equations are also changed from (1), (2) and (3) to (23), (24) and (25) or (39). This change results in the sudden impulses in solid because there is no impedance term in the governing equations of supersolid and the amplitudes of velocity and temperature on the side of regular solid will be magnified on the side of supersolid. This train of impulses is conveniently expressed by the so-called Dirac combs. For example, if we assume that

We assume that there is a displacement perturbation on the regular solid side,

$$\xi^{\dagger} = \xi_0^{\dagger} \sin(2\pi f k_2 x) \sin(2\pi f k t) = \varphi(x, y)\alpha_k(t) \tag{40}$$

where $\xi^{\dagger}$ is the displacement and $\xi_0^{\dagger}$ is the corresponding amplitude of displacement. Superscript † is used to specify variables on the regular solid side. According to (6) and (7),

$$\Lambda = \Lambda_{ij} = \frac{1}{2}\left(\frac{\partial u_i}{\partial x_j} + \frac{\partial u_j}{\partial x_i}\right) = \pi f k \left(\frac{\partial \varphi}{\partial x} + \frac{\partial \varphi}{\partial y}\right) \cos(2\pi f k t) \tag{41}$$

$$E = E_{ij} = \frac{1}{2}\left(\frac{\partial \xi_i}{\partial x_j} + \frac{\partial \xi_j}{\partial x_i}\right) = \frac{1}{2}\left(\frac{\partial \varphi}{\partial x} + \frac{\partial \varphi}{\partial y}\right)\alpha_k(t) = \frac{1}{2}\left(\frac{\partial \varphi}{\partial x} + \frac{\partial \varphi}{\partial y}\right) \sin(2\pi f k t) \tag{42}$$

To guarantee the second term on the right of (17) is zero,

$$E: \Lambda = \frac{\pi f k}{2}\left(\frac{\partial \varphi}{\partial x} + \frac{\partial \varphi}{\partial y}\right)^2 \sin(2\pi f k t)\cos(2\pi f k t) = 0 \tag{43}$$

we shall have

$$\sin(2\pi f k t)\cos(2\pi f k t) = 0 \tag{44}$$

By assuming $f = k = 1$, we illustrate the temporal terms in (40), (42), (44) and velocity (45),

$$u^{\dagger} = \frac{d\xi^{\dagger}}{dt} = u_0^{\dagger}\cos(2\pi f k t) \tag{45}$$

where $u_0^{\dagger} = 2\pi\xi_0^{\dagger}$ and it should be noted that we apply the derivative only to one period; hence the velocity is replicated through compound frequency fk, not amplified. At $t = 0, 0.25, 0.5, 0.75, 1.0$, the function $\sin(2\pi f k t)\cos(2\pi f k t)$, marked by the solid thick curve, is zero and they are on the boundary of the second law and solid parcels become supersolid. At $t = 0.25\ and\ 0.75$, the corresponding velocity of the solid parcel is zero; then, the velocity of solid passing onto supersolid is null. At $t = 0, 0.5, 1.0$, the corresponding velocity of the regular solid parcels are at the extrema, marked by the thick arrowed lines, and at $t = 0, 1.0$, the velocity has the maximum and at $t = 0.5$, the velocity has the minimum.

At $t = 0, 0.5, 1.0$, the solid becomes supersolid and the governing equations are changed from (1), (2), (3) to (39) and supersolid experiences velocity impulses $+u_0^{\dagger}$ and $-u_0^{\dagger}$, which are given in the Dirac combs

$$\text{ṁ}_1\ (t) = u_0^{\dagger}\sum_1^K \delta(t - k + 0) \tag{46}$$

$$\text{ṁ}_2\ (t) = -u_0^{\dagger}\sum_1^K \delta(t - k + 0.5) \tag{47}$$

where ṁ_1 and ṁ_2 represent the Dirac comb in positive impulses and negative impulses by the dark lines with arrows in Fig. 1. At a given frequency

$$f = \frac{k}{\lambda} \tag{48}$$

where k is the wavenumber and λ is the period. The Fourier transformation of (66) and (67) with the spacing $\frac{2\pi\lambda}{k}$,

$$\text{ṁ}_1\ (k) = \frac{1}{2\pi}u_0^{\dagger}\sum_{k=1}^K f\delta(k) \tag{49}$$

$$\text{ṁ}_2\ (k) = -\frac{1}{2\pi}u_0^{\dagger}\sum_{k=1}^K f\delta(k) \tag{50}$$

which yields the Fourier coefficients for the Dirac combs,

$$s_1(k) = \frac{1}{2\pi}u_0^{\dagger} f \tag{51}$$

$$s_2(k) = -\frac{1}{2\pi}u_0^{\dagger} f \tag{52}$$

Now, we work on the boundary conditions. For simplicity, we assume a one-dimensional problem as indicated by (40). Recall that to satisfy the conditions that the excess entropy becomes zero by (16), (43) must be guaranteed or

$$\left(\frac{\partial \varphi}{\partial x}\right)^2 \sin(2\pi f k t)\cos(2\pi f k t) = 0 \tag{53}$$

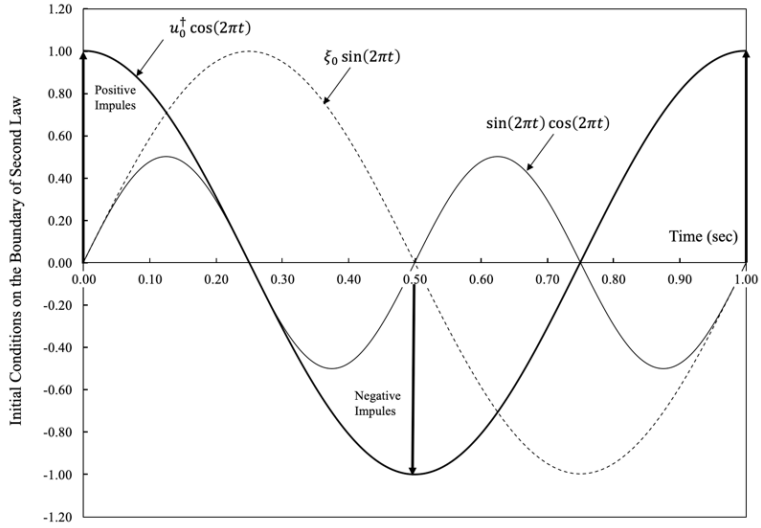

Figure 1: Initial conditions on the boundary of the second law.

We have discussed the temporal conditions for the initial conditions of the part in (53), $\sin(2\pi fkt)\cos(2\pi fkt)$. The velocity can be expressed by the spatial distribution from (45),

$$u^\dagger = \frac{d\xi^\dagger}{dt} = u_0^\dagger \sin(2\pi f k_2 x)\cos(2\pi fkt) \tag{54}$$

The spatial function $\left(\frac{\partial\varphi}{\partial x}\right)^2$ can also be nullified just like the temporal component from (53),

$$\left(\frac{\partial\varphi}{\partial x}\right)^2 = [2\pi f k_2 \cos(2\pi f k_2 x)]^2 = 0 \tag{55}$$

The physical meaning of (54) and (55) can be visualised in Fig. 2. For convenience, we divided the spatial dimension by a nominal dimension to keep x dimensionless and assume a constant period of 2π. There are two curves representing the velocity (54) and dissipation term in the excess entropy eqn (55). At $x = 0.25, 0.75$, there are two points that the dissipation spatial term intercepts with the horizontal axis, which means that at these two points, the excess entropy is zero and locally, the nondissipative thermodynamic state has been observed. At $x = 0.25, 0.75$, the resonant solid is adjacent to the regular solid, which shall hold the velocity quite close to the peak of the space if we are only concerned with the local velocity. This resonant solid parcel surrounded by the regular solid; hence the velocity of the regular solid is used to assign the boundary conditions of the resonant supersolid at $x = 0.25, 0.75$. From Fig. 2, we can see that at $x = 0.25$, the velocity is positive while at $x = 0.75$, the velocity is negative. If we consider continuously the displacement function (40), the positive and negative impulses can be treated with the Dirac combs as we have done to the initial conditions (46) and (47).

$$\text{ṁ}_{1x}(x) = u_0^\dagger \sum_1^{K_2} \delta(x - k_2 + 0.25) \tag{56}$$

$$\text{ṁ}_{2x}(x) = -u_0^\dagger \sum_1^{K_2} \delta(x - k_2 + 0.75) \tag{57}$$

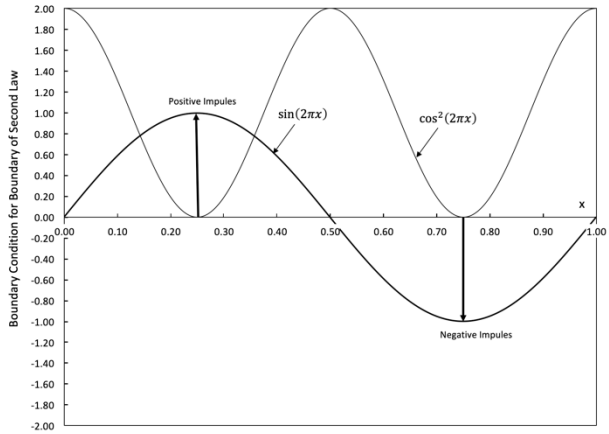

Figure 2: Boundary conditions on the boundary of the second law.

The initial conditions (46), (47) and boundary conditions (56), (57) are antinodes of the resonance and contribute to the resonance and sustain the spatiotemporal nondissipative dynamics. On the other hand, the points in the space where the velocity is zero are nodes. According to Figs 1 and 2, the nodes in space and time from the displacement function (40) are dissipative since they do not comply to the condition of the boundary of the second law. Actually, a node can be dissipative or nondissipative depending on if they are on the boundary of the second law.

In this section, we have established the initial and boundary conditions for the velocity of the resonant supersolid. In the next section, we will apply the initial and boundary conditions to determine the velocity field of the resonant supersolid.

4 VELOCITY DISTRIBUTION

In this section, we solve a one-dimensional spatiotemporal velocity field of resonant supersolid and the velocity field will be validated with the experimental data in the next section.

In the preceding sections, we derive the governing equations of nondissipative, resonant solids from the governing equations of dissipative, regular solid. Here, we must pause temporarily in order to clarify several critical concepts and differentiate them from the conventional meanings in theoretical physics and the theory of partial differential equations. First, the nondissipative motions here is fundamentally distinct from the nondissipative system in the theoretical physics [35], [36]. In the theory of excess entropy, the nondissipative motion is the real solid motion at the isentropic thermodynamic state and the nondissipative and dissipative solids are dependent of each other. Moreover, the real solid nondissipative motion can be excited into resonance and generate sound. Since it experiences the impulsively initial and boundary conditions, the real nondissipative process is irreversible. Finally, the real, nondissipative, resonant solid follows (39), which is completely different from that of the dissipative solid. The mathematical formulation of the nondissipative system of a solid is usually considered the degenerate partial differential equations of the partial differentiate equations of a dissipative system [37], [38]. Strongly associated with the degenerate partial differential equations, the singularity of the governing equations of an isotropic Hookean solid occurs at so-called ‘vanishing dissipation’ conditions [39], [40]. It is

arguable that the governing differential equations of the nondissipative solid are degenerate equations at the 'vanishing dissipation' singularity. The question has been raised on whether the dissipative partial differential equation has already included the nondissipative equations; therefore, the solutions of the motions of the dissipative solids also include those of the nondissipative solids. The rebuttal on this point of view is demonstrated by the derivation and validation cases in this work. In another word, the solution of the degenerate partial differential equations of the nondissipative motions cannot be elaborated by the original partial differential equations.

In this work, we will solve one-dimensional resonant supersolid and compare it with the experimental data. From (39), the one-dimensional partial differential equation for resonant, supersolid is given below,

$$\frac{\partial u}{\partial t} + c_1 \frac{\partial u}{\partial x} = -\frac{1}{\rho}\frac{\partial p}{\partial x} \tag{58}$$

Eqn (58) is a first-order, inhomogeneous partial differential equation and can be written as

$$u = u_h + u_p \tag{59}$$

where u_h and u_p are the general solution of the homogeneous differential equation and the particular solution of the inhomogeneous part, respectively. Application of the separation method to the homogeneous differential eqn (59),

$$u_h = \mathrm{A(t)B(x)} \tag{60}$$

Bring (60) to (58),

$$\mathrm{B}\frac{d\mathrm{A}}{dt} + c_1 \mathrm{A}\frac{d\mathrm{B}}{dx} = 0 \tag{61}$$

Divide (61) by (60),

$$\frac{1}{A}\frac{dA}{dt} + \frac{c_1}{B}\frac{dB}{dx} = 0 \tag{62}$$

Since each term in (62) are functions of time and space only, we can write them in the eigenfunctions,

$$n_1 + n_2 = 0 \tag{63}$$

where n_i, $i = 1,2$ are the complex eigenvalues, expressed by

$$\begin{cases} n_1 = (\alpha_1 + if_1)k_1 \\ n_2 = (\alpha_2 + if_2)k_2 \end{cases} \tag{64}$$

where α_i, f_i and k_i are amplitude factors, frequency factors and harmonics of time and space for velocity respectively. From (63) and (64), n_i, α_i, f_i and k_i are not all independent variables.

From the definition of eigenvalues (63) and (64),

$$\frac{1}{A}\frac{dA}{dt} = -n_1, \frac{c_1}{B}\frac{dB}{dx} = -n_2 \tag{65}$$

we have the general solutions,

$$u_h = \sum_{k_1=1}^{K_1}\sum_{k_2=1}^{K_2} A_0 B_0 e^{-(\alpha_1+if_1)k_1 t} e^{-\frac{(\alpha_2+if_2)}{c_1}k_2 x} \tag{66}$$

where A_0 and B_0 are the constants to be determined by the boundary conditions. If it is known, the pressure in (58) can be expanded into series along the kernel of the homogeneous solutions (66),

$$p = \sum_{k_1=1}^{K_1} \sum_{k_2=1}^{K_2} p_A p_B e^{-(\alpha_1 + i f_1) k_1 t} e^{-\frac{(\alpha_2 + i f_2)}{c_1} k_2 x} \tag{67}$$

By assuming the particular solution in (59) has the form of

$$u_p = \sum_{k_1=1}^{K_1} \sum_{k_2=1}^{K_2} A_p B_p e^{-(\alpha_1 + i f_1) k_1 t} e^{-\frac{(\alpha_2 + i f_2)}{c_1} k_2 x} \tag{68}$$

We can determine the coefficients A_p and B_p in (68) by the coefficients p_A and p_B through (67); otherwise, we can iterate to obtain A_p and B_p numerically, which implies that we can express the solution of velocity by

$$u = \sum_{k_1=1}^{K_1} \sum_{k_2=1}^{K_2} A_s B_s e^{-(\alpha_1 + i f_1) k_1 t} e^{-\frac{(\alpha_2 + i f_2)}{c_1} k_2 x} \tag{69}$$

where $A_s B_s = A_0 B_0 + A_p B_p$.

We call (69) for velocity the general solution of the resonant supersolid. When $\alpha_1 = 0$ and $\beta_1 = 0$, we obtain the quasi-steady-state solution of temperature and velocity,

$$u = \sum_{k_1=1}^{K_1} \sum_{k_2=1}^{K_2} A_s B_s e^{-i f_1 k_1 t} e^{-\frac{(\alpha_2 + i f_2)}{c_1} k_2 x} \tag{70}$$

Therefore, the quasi-steady-state motion (70) in the resonant supersolid consists of sinusoidal and cosinusoidal waves.

Next, we rearrange (70) so that they are explicit functions of time only and prepare to apply the boundary conditions in the next section. We first look at terms in (70),

$$\begin{aligned} & e^{-(\alpha_1 + i f_1) k_1 t} e^{-\frac{(\alpha_2 + i f_2)}{c_1} k_2 x} \\ & = e^{-\alpha_1 k_1 t} (\cos f_1 k_1 t + i \sin f_1 k_1 t) e^{-\frac{\alpha_2}{c_1} k_2 x} \left(\cos \frac{f_2}{c_1} k_2 x + i \sin \frac{f_2}{c_1} k_2 x \right) \\ & = e^{-\alpha_1 k_1 t} e^{-\frac{\alpha_2}{c_1} k_2 x} \left(\cos f_1 k_1 t \cos \frac{f_2}{c_1} k_2 x - \sin f_1 k_1 t \sin \frac{f_2}{c_1} k_2 x + i \cos f_1 k_1 t \sin f_1 k_1 t + \right. \\ & \left. i \sin f_1 k_1 t \cos \frac{f_2}{c_1} k_2 x \right) \end{aligned} \tag{71}$$

By grouping and taking the real terms in (71), the velocity is the explicit function of time,

$$u = \sum_{k_1=1}^{K_1} \sum_{k_2=1}^{K_2} \left(\varphi_{1,k} \cos f_1 k_1 t \cos \frac{f_2}{c_1} k_2 x - \varphi_{2,k} \sin f_1 k_1 t \sin \frac{f_2}{c_1} k_2 x \right) e^{-\alpha_1 k_1 t} e^{-\frac{\alpha_2}{c_1} k_2 x} \tag{72}$$

where $\varphi_{1,k}$ and $\varphi_{2,k}$ are implicit functions of the coefficients A_s, B_s, f_i, α_i and k_i, $i = 1,2$. (72) can be written in dependent of t and x respectively,

$$u = \sum_{k_1=1}^{K_1} \left(\Phi_{1,k} \cos f_1 k_1 t - \Phi_{2,k} \sin f_1 k_1 t \right) e^{-\alpha_1 k_1 t} \tag{73}$$

and

$$u = \sum_{k_2=1}^{K_2} \left(\Omega_{1,k} \cos \frac{f_2}{c_1} k_2 x - \Omega_{2,k} \sin \frac{f_2}{c_1} k_2 x \right) e^{-\frac{\alpha_2}{c_1} k_2 x} \tag{74}$$

where $\Phi_{1,k} = \sum_{k_2=1}^{K_2} \varphi_{1,k} \cos \frac{f_2}{c_1} k_2 x \, e^{-\frac{\alpha_2}{c_1} k_2 x}$, $\Phi_{2,k} = \varphi_{2,k} \sin \frac{f_2}{c_1} k_2 x$,

$\Omega_{1,k} = \sum_{k_1=1}^{K_1} \varphi_{1,k} \cos f_1 k_1 t \, e^{-\alpha_1 k_1 t}$, and $\Omega_{2,k} = \varphi_{2,k} \sin f_1 k_1 t \, e^{-\alpha_1 k_1 t}$.

We apply the Fourier transformation to (56) and (73), we obtain

$$\frac{1}{2\pi k_1 f_1} u_0^\dagger = \int_0^\infty \left(\Phi_{1,k} \cos 2\pi k_1 f_1 t - \Phi_{2,k} \sin 2\pi k_1 f_1 t\right) e^{-2\pi\alpha_1 k_1 t} \cos 2\pi k_1 f_1 t \, dt \quad (75)$$

$$-\frac{1}{2\pi k_1 f_1} u_0^\dagger = \int_0^\infty \left(\Phi_{1,k} \cos 2\pi k_1 f_1 t - \Phi_{2,k} \sin 2\pi k_1 f_1 t\right) e^{-2\pi\alpha_1 k_1 t} \sin 2\pi k f_k t \, dt \quad (76)$$

Since $\Phi_{1,k}$ and $\Phi_{2,k}$ are not the function of time, the integration in (75) and (76) can be expressed by an algebraic equation

$$\begin{cases} \mathrm{M}_1 \Phi_{1,k} - \mathrm{M}_2 \Phi_{2,k} = \frac{1}{2\pi k_1 f_1} u_0^\dagger \\ \mathrm{M}_2 \Phi_{1,k} - \mathrm{M}_3 \Phi_{2,k} = -\frac{1}{2\pi k_1 f_1} u_0^\dagger \end{cases} \quad (77)$$

where

$$M_1 = \int_0^\infty \cos 2\pi k_1 f_1 t \, e^{-2\pi\alpha_1 k_1 t} \cos 2\pi\alpha_1 k_1 t \, dt = \frac{2f_1^2 + \alpha_1^2}{2\pi\alpha_1 k_1 \left(4f_1^2 + \alpha_1^2\right)}$$

$$M_2 = \int_0^\infty \sin 2\pi k_1 f_1 t \, e^{-2\pi k_1 f_1 t} \cos 2\pi k_1 f_1 t \, dt = \frac{2f_1\alpha_1}{4\pi\alpha_1 k_1 \left(4f_1^2 + \alpha_1^2\right)}$$

$$M_3 = \int_0^\infty \sin 2\pi k_1 f_1 t \, e^{-2\pi k_1 f_1 t} \sin 2\pi k_1 f_1 t dt = \frac{4f_1^2}{4\pi\alpha_1 k_1 \left(4f_1^2 + \alpha_1^2\right)} \quad (78)$$

Solve (78),

$$\Phi_{1,k} = \frac{\alpha_1(\alpha_1 + 2f_1)}{f_1^2} u_0^\dagger \quad (79)$$

$$\Phi_{2,k} = \frac{\alpha_1\left[\left(2f_1^2 + \alpha_1^2\right) + f_1\alpha_1\right]}{f_1^3} u_0^\dagger \quad (80)$$

Following the same procedure, we can obtain the integral constants for the spatial dimension,

$$\Omega_{1,k} = \frac{\alpha_2(\alpha_2 + 2f_2)}{f_2^2} \quad (81)$$

$$\Omega_{2,k} = \frac{\alpha_2\left[\left(2f_2^2 + \alpha_2^2\right) + f_2\alpha_2\right]}{f_2^3} \quad (82)$$

Therefore, we obtain the velocity in one-dimensional, resonant solid,

$$u = u_0^\dagger \sum_{k_1=1}^{K_1} \sum_{k_2=1}^{K_2} \left(\frac{\alpha_1(\alpha_1 + 2f_1)}{f_1^2} \frac{\alpha_2(\alpha_2 + 2f_2)}{f_2^2} \cos 2\pi f_1 k_1 t \cos 2\pi \frac{f_2}{c_1} k_2 x - \frac{\alpha_1\left[\left(2f_1^2 + \alpha_1^2\right) + f_1\alpha_1\right]}{f_1^3} \frac{\alpha_2\left[\left(2f_2^2 + \alpha_2^2\right) + f_2\alpha_2\right]}{f_2^3} \sin 2\pi f_1 k_1 t \sin 2\pi \frac{f_2}{c_1} k_2 x\right) e^{-2\pi\alpha_1 k_1 t} e^{-2\pi\frac{\alpha_2}{c_1} k_2 x} \quad (83)$$

In summary, we have derived the one-dimensional, temporal velocity distribution for the resonant supersolid, which is the function of the amplitude of perturbation velocity, frequency and amplitude factors and harmonics in both spatial and temporal directions. We will validate the velocity field in the next section by experimental data.

5 VALIDATION

In this section, we proceed to validate the velocity distribution (83). The purpose of the validation is to demonstrate that at the interface of two solids, the supersolid occurs and dominates the essential behaviours at the interfaces. The velocity distribution derived is

applicable to any kind of load and especially to the engineering and manufacture scenarios. Because the propensity of nondissipative processes at the interfaces, we believe that most of damages observed belong to this category, which cannot be predicted properly with mesh refinement and with dissipative motions only. On the contrary, if we include the nondissipative dynamics properly, the physics of interfaces is more comprehensive and the demand on the numerical parameters such as mesh and time steps etc. are more relaxed with higher or equivalent accuracy.

Obviously, there are vast of experimental cases on the interfacial phenomena between solids and a recent study on the ballistic heat transfer at the solid interface has applied the nondissipative dynamic theory [27]. Consequently, we may want to choose the experiments on the strain or strain rate at an interface. The experiments on the frictional sliding modes on the interface on two identical elastic plates seem to cover a wide range of parametric factors and provide both visual and quantitative observation and measurements [41]–[44].

The tests were conducted on the interface of two plates of the same kind of solid, Homalite-100, a brittle polyester resin. The plates are 76.2 mm long, 139.7 mm wide and 9.525 mm thick, which is the contact side of the plates. A nominal pressure is applied on two plates perpendicular to the interface. The impact loading from as cylindrical steel projectile of diameter 25 mm and length 51 mm, fired from a gas gun at various speed before hitting the plate. The loading wave is measured by a strain gage glued to the specimen. Dynamic photoelasticity is used to extract stress field around the interface. The photoelastic fringe patterns were recorded in real time using a high-speed camera capable of capturing 16 images at a rate of 16 images of 100 million frames. Two pairs of polariser plates are placed on either side of the Homalite plates that generate isochromatic fringes. The isochromatic fringes are interpreted to the contours of stresses $\sigma_1 - \sigma_2$, with σ_1 the maximum in-plane principal stress and $\sigma_2$the minimum in-plane principal stress. The testing results with two operating parameters, the pressure and impact velocity, are published.

At the instant of the impact, the interface is usually assumed to move slightly and then stops due to the friction. However, it has been observed that plate may slide along the interface substantially. The physics of this sliding is unclear and therefore, there is no mathematical representation on the sliding profile. However, it serves a good example to demonstrate the physics of nondissipative dynamics when we can properly present the velocity profiles since the supersolid has no resistance on shear. We use this example to illustrate that supersolid and resonant supersolid are dominate on the interface phenomena.

The contours of infringe show that there are about five different distinct modes, a crack-like mode, a pulse-like mode, a train of pulses, multiple pulses coalescing, and a pulse-like mode followed by a crack-like mode. All of these five modes can be classified by the velocity or the strain rate of stress and strain waves. The benchmark test was conducted by producing the impact on both plates and a high-speed wave is observed at the interface, which creates also a shock line defined by the first sound. This clearly indicates that the interface went into resonant supersolid mode, which leads to the understanding of the five modes. The crack-like mode is dominated by supersolid. The pulse-like mode is a soliton due to the resonant of supersolid and the resonant is very local and limited to the interface. The pulse-like train is the resonant supersolid mode that has over-spilt onto the adjacent solid and the resonance sustains for a longer duration in time and space. The multiple pulses coalescing to form a crack is when the resonance is in the transition into non-resonance mode. A pulse-like mode followed by a crack-like mode is also a transition mode from strong resonance to a broad band resonance or non-resonance mode.

The pulse-like train is probably a relative stable resonance mode. The temporal component behaves as chaos or turbulence and the spatial component visualises by the isochromatic infringes. In this work, we apply the mathematical solution (83) of the velocity field to model the pulse-like train. For a spatial distribution, only the spatial terms in (83) show up

$$u = u_0^{\dagger} \sum_{k_2=1}^{K_2} \alpha_2 \left(\frac{\alpha_2 + 2f_2}{f_2^2} \cos 2\pi f_2 k_2 x - \frac{(2f_2^2 + \alpha_2^2) + f_2 \alpha_2}{f_2^3} \sin 2\pi f_2 k_2 x \right) e^{-2\pi \alpha_2 k_2 x} \quad (84)$$

Note that for convenience, we replace $\frac{f_2}{c_1}$ and $\frac{\alpha_2}{c_1}$ by f_2 and α_2. When we apply the parameters in Table 1, the agreement is satisfactory in Fig. 3. The data shows that the pulses are not generally symmetric. Since it is the in-plane velocity, the velocity in the positive axial dimension is slightly higher than that in the negative axial direction probably from the overall motion is in the positive direction. The published data is somewhat 'translated' from the isochromatic infringes by the finite element simulation and the translation may result in some losses of the subtle information. For example, near the location where the velocity becomes zero, the data shows a sharp turn to zero but (84) continues to extend into the negative for some nominal values and then comes back eventually. In the chaotic distribution, this negative region has been measured if we allow a non-zero baseline of velocity field. This non-zero velocity base is consistent to the asymmetric velocity profile as we have pointed before.

Table 1: Parameters for the velocity distribution.

Parameter	u_0 (m/s)	α_2	f_2	k_2
Value	3.096	0.210	0.040	1

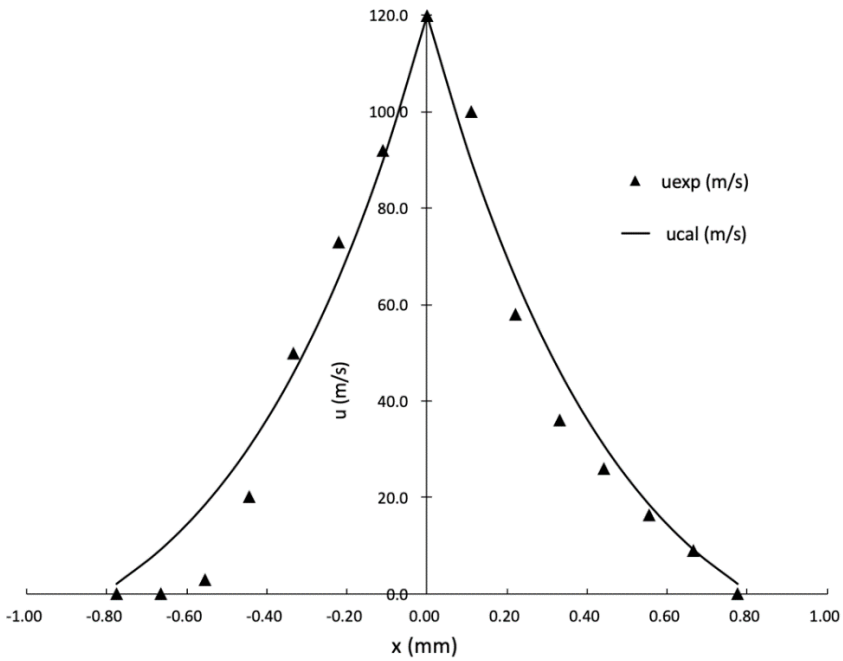

Figure 3: Experimental and calculated pulse in a pulse train at the interface.

The pulse-like train consists of a series of pulses in the space and the theory says that the temporal and spatial parts (44) and (54) of the oscillatory loads both reach zero simultaneously. The solution has temporal and spatial parts (83) and the spatial parts has the nodal and antinodal points where the velocity becomes zero or maximum and minimum. Those spatial pulses are the antinodal locations and the antinodal locations into the volumetric domains in each plate can be seen in the isochromatic infringes and the computed infringe patterns.

In Fig. 4, we plot the antinodes according to the experimental spacing. The jump from the transition of the thermodynamic states is observed from the magnitude of the perturbation velocity $u_0 = 3.096$ m/s to $u_{max} = 120$ m/s from Table I. Physically, the interface has higher propensity to form resonance supersolid, which is inherently from the fact that there is geometric morphology at contact that easily satisfies the requirements on the spatial condition (54). As soon as there is a temporal wave passing through, those spatial morphologies shall form the waves in space and excites the interfaces.

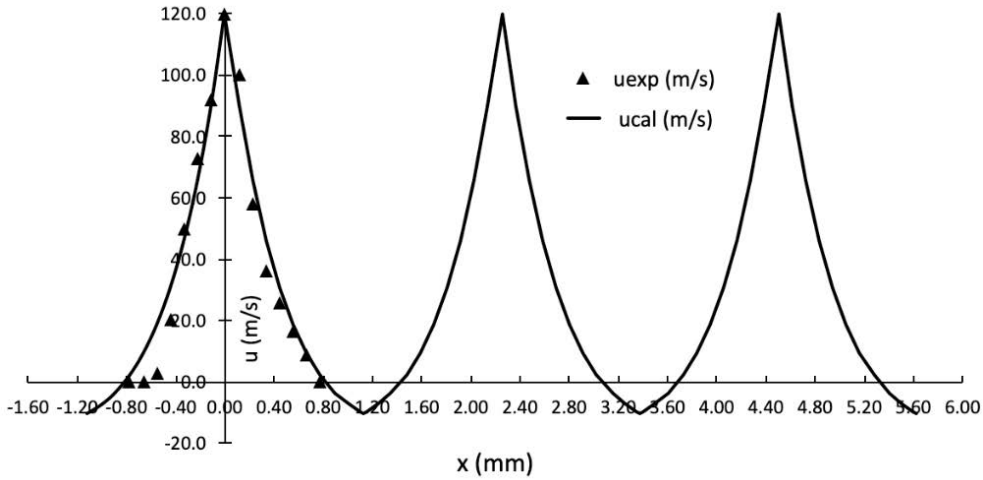

Figure 4: A pulse train at the interface.

6 CONCLUSIONS

In this work, we introduce the nondissipative dynamics in solids to solve the interface problem of in-plane velocities. The process, the governing differential equations and the solutions of nondissipative motions show that at interface, the nondissipative dynamics is a common phenomenon.

The purposes of this demonstration are two folds. First, the interfacial strain and deformation are mainly from the motion of nondissipative dynamics and can only be properly counted by the introduction of the nondissipative dynamics. This finding should greatly relax the demand on the boundary element method and the formulation of the nondissipative dynamics, sliding and topologies can be included in the integration equations of the boundary element method.

Second, the formulation of velocity and displacements at interfaces can be calculated by (83). The calculation of the nondissipative dynamics should be performed with the dissipative solid mechanics.

ACKNOWLEDGEMENTS

The authors are grateful for the support of the Beijing Natural Science Foundation IS23027.

REFERENCES

[1]
[2] Popov, V.L., *Contact Mechanics and Friction, Physical Principles and Applications*, Springer: Berlin, 2010.
[3] Burger, H., Forsbach, F. & Popov, V.L., Boundary element method for tangential contact of a coated elastic half-space. *Machines*, **11**(694), pp. 1–15, 2023.
[4] Komvopoulos, K., A multiscale theoretical analysis of the mechanical thermal, and electrical characteristics of rough contact interfaces demonstrating fractal behavior. *Frontiers in Mechanical Engineering*, **6**(36), pp. 1–20, 2020.
[5] Chen, J., Xu, X., Zhou, J. & Li, B., Interfacial thermal resistance: Past, present, and future. *Reviews of Modern Physics*, **94**, 025002, 2022.
[6] Stoner, R. & Maris, H., Kapitza conductance and heat flow between solids at temperatures from 50 to 300 K. *Physical Review B*, **48**(22), pp. 16373–16387, 1993.
[7] Swartz, E. & Pohl, R., Thermal boundary resistance. *Reviews of Modern Physics*, **61**, p. 605, 1989.
[8] Cahill, D.G. et al., Nanoscale thermal transport II: 2003–2012. *Applied Physics Reviews*, **1**, 011305, 2014.
[9] Ransom, J.B., McCleary, S.L. & Aminpour, M.A., A new finite element for connecting independently modeled substrates. *AIAA/ASME/ASCE/AHS/ASC Structures, Structural Dynamics/Material Conference*, 1993.
[10] D'Andrea, A., Tozzo, C., Boschetto, A. & Bottini, L., Interface roughness parameters and shear strength. *Modern Applied Science*, **7**(10), pp. 1–10, 2013.
[11] Kapitza, P., The study of heat transfer in helium II. *J. Phys. USSR*, **4**, p. 181, 1941.
[12] Landau, L., Theory of the superfluidity of helium II. *J. Phys. USSR*, **5**, pp. 301–330, 1941.
[13] Gol'danskii, V., Trakhtenberg, L. & Fleurov, V., *Tunneling Phenomena in Chemical Physics*, Taylor and Francis: New York, 2021.
[14] Su, S., Zhang, Y., Chen, J. & Shih, T.-M., Thermal electron-tunneling devices as coolers and amplifiers. *Nature Scientific Reports*, **6**, 21425, 2016.
[15] Bramble, J.H. & King, J.T., A finite element method for interface problems in domains with smooth boundaries and interfaces. *Advances in Computational Mathematics*, **6**, pp. 109–138, 1996.
[16] Aminpour, M.A., Krishnamurthy, T. & Shin, Y., Coupling of independent modeled three-dimensional finite element meshes with non-matching arbitrary shape interface boundaries. *AIAA Conference*, 1999.
[17] Fadale, T.D. & Aminpour, M.A., Thermal interface element for independently modeled finite element meshes. *AIAA Structures, Structural Dynamics/Material Conference*, 1999.
[18] Cheng, A.H.-D. & Cheng, D.T., Heritage and early history of the boundary element method. *Engineering Analysis with Boundary Elements*, **26**, pp. 268–302, 2005.
[19] Gipson, G.S., Issues related to interface calculations in the boundary element method. *Transactions on Modelling and Simulations*, 1999.
[20] Huang, D., Yan, X., Larsson, R. & Almqvist, A., Boundary element method for the elastic contact problem with hydrostatic load at the contact interface. *Applied Surface Science Advances*, **6**, 100176, 2021.

[21] Tan, C. & Gao, Y., Treatment of bimaterial interface crack problems using the boundary element method. *Engineering Fracture Mechanics*, **36**(6), pp. 919–932, 1990.
[22] Hutchings, I.M., Leonardo da Vinci's studies of friction. *Wear (Supplement C)*, **360**, pp. 51–66, 2016.
[23] Archard, J., Contact and rubbing of flat surfaces. *Journal of Applied Physics*, **24**(8), pp. 981–988, 1953.
[24] Earies, S. & Lee, C., Instabilities arising from the friction interaction of a pin-disk system resulting in noise generation. *Journal of Engineering for Industry*, **98**(1), pp. 81–86, 1976.
[25] Prakash, V., Frictional response of sliding interfaces subjected to time varying normal pressures. *Journal of Tribology*, **120**, pp. 97–102, 1998.
[26] Gupta, A. & Gupta, A.K., Missing mass effect in coupled analysis I: Complex modal properties. *Journal of Structural Engineering*, **124**(5), pp. 490–495, 1998.
[27] Oden, J. & Pires, E., Nonlocal and nonlinear friction laws and variational principles for contact problems in elasticity. *Journal of Applied Mechanics*, **50**, pp. 67–73, 1983.
[28] Chen, W., Hydrodynamic heat transfer in solids. *International Journal of Heat and Mass Transfer*, **215**, 124455, 2023.
[29] Malvern, L.E., *Introduction to the Mechanics of a Continuous Medium*, Prentice-Hall: Englewood, 1969.
[30] Bertram, A. & Gluge, R., *Solid Mechanics, Theory, Modeling and Problems*, Springer: Heidelberg, 2015.
[31] Chen, W., Heat transfer at speed of sound. *International Journal of Heat and Mass Transfer*, **177**, 121529, 2021.
[32] Chen, W., Heat transfer at speed of sound. *International Journal of Heat and Mass Transfer*, vol. **177**, pp. 1–13, 2021.
[33] Leggett, A., Can a solid be 'superfluid'? *Physical Review Letters*, **25**(22), pp. 1543–1546, 1970.
[34] Balibar, S. & Caupin, F., Supersolidity and disorder. *Journal of Physics on Condense Matters*, 20, 173201, 2008.
[35] Chen, W., On Taylor correlation functions in isotropic turbulent flows. *Nature Scientific Reports*, **13**(3859), pp. 1–31, 2023.
[36] Shimizu, T., Constants of the motion in nondissipative and dissipative systems. *Progress of Theoretical Physics*, **47**(4), pp. 1181–1199, 1972.
[37] Silva, R.P.d., Non-dissipative system as limit of a dissipative one: comparison of the asymptotic regimes. *Bulletin of the Brazilian Mathematical Society, New Series*, **51**, pp. 125–137, 2020.
[38] Chen, G.-Q.G., On degenerate partial differential equations. arXiv:1005.2713v1, **5**, pp. 1–39, 2010.
[39] Debussche, A., Hofmanova, M. & Vovelle, J., Degenerate parabolic stochastic partial differential equations: Quasilinear case. *The Annals of Probability*, **44**(3), pp. 1916–1955, 2016.
[40] Ivanov, A., On singularity points of equations of mechanics. *Doklady Mathematics*, **97**(2), pp. 167–169, 2018.
[41] Zhou, Y. & Gupta, V., Interface solutions of partial differential equations with point singularity. *Journal of Computational and Applied Mathematics*, **362**, pp. 400–409, 2019.

[42] Coker, D., Lykotrfitis, G., Needleman, A. & Rosakis, A., Frictional sliding modes along an interface between identical elastic plates subject to shear impact loading. *Journal of the Mechanics and Physics of Solids*, **53**(1), pp. 884–922, 2005.
[43] Lykotrafitis, G., Rosakis, A.J. & Ravichandran, G., Self-healing pulse-like shear rupture in the laboratory. *Science*, **313**, pp. 1765–1768, 2006.
[44] Rosakis, A., Samudrala, O. & Coker, D., Cracks faster than the shear wave speed. *Science*, **284**, pp. 1337–1340, 1999.
[45] Rosakis, A.J., Samudrala, O. & Coker, D., Intersonic shear crack growth along weak planes. *Materials Research Innovations*, **3**, pp. 236–243, 2000.